JOURNAL OF GEOPHYSICAL RESEARCH, VOL. 117, G02012, doi:10.1029/2011JG001899, 2012

A model-based evaluation of woody plant encroachment effects on coupled carbon and water cycles

F. C. O'Donnell[1] and K. K. Caylor[1]

Received 28 October 2011; revised 2 March 2012; accepted 10 March 2012; published 4 May 2012.

[1] The conversion of grasslands to shrublands by woody plant encroachment is a common occurrence in arid and semi-arid regions that can have significant effects on ecosystem hydrology and biogeochemistry, including changes in soil organic carbon stocks. The mechanisms determining the direction and magnitude of soil carbon change due to encroachment are unknown but appear to depend on factors that vary along a gradient of mean annual precipitation. We present a model of coupled steady-state soil moisture and carbon dynamics that accounts for the effects of structural heterogeneity at the scale of vegetation patches by representing the local effects of root systems and canopies. We applied the model to paired grasslands and woody encroachment-produced shrublands spanning a climate gradient in the American Southwest, and model results were consistent with measured values. Modeled transpiration, which was used to determine productivity, was 5%–57% greater in shrublands, with the greatest difference occurring where the relative difference in leaf area index between grass and shrub patches was small and vegetation density was low. Patterns of soil carbon abundance were mainly driven by patterns of productivity, but decomposition rates were also affected by vegetation structure. Woody encroachment increases heterogeneity in soil carbon decomposition rates and has the net effect of increasing soil carbon residence times by 3.6–4.9 years. Our model represents an important step toward a mechanistic and quantitative understanding of the effect of vegetation structure on soil moisture and carbon dynamics and highlights the need for a better description of belowground vegetation structure in ecosystem models.

Citation: O'Donnell, F. C., and K. K. Caylor (2012), A model-based evaluation of woody plant encroachment effects on coupled carbon and water cycles, *J. Geophys. Res.*, *117*, G02012, doi:10.1029/2011JG001899.

1. Introduction

[2] Woody plant encroachment into grass-dominated landscapes is common and well-documented in dryland regions [*Archer et al.*, 1995; *House et al.*, 2003]. It is attributed to a number of factors including climate change, CO_2 fertilization, overgrazing, and fire suppression [*Archer et al.*, 1995; *Van Auken*, 2000; *Morgan et al.*, 2007; *Knapp et al.*, 2008] that are likely to increase in the future, making it important to understand the impact of woody encroachment on ecosystem functions and services. Drylands, which cover 40% of the global land surface, account for around 30% of global terrestrial net primary productivity [*Grace et al.*, 2006], with a high fraction of biomass in belowground pools [*Schenk and Jackson*, 2002]. The impact of woody encroachment on dryland carbon stocks and fluxes is poorly understood, leading to uncertainties in projections of future regional and global carbon budgets [*Goodale and Davidson*, 2002; *Woodbury et al.*, 2007].

[3] A number of studies have observed significant changes in soil carbon stocks following woody encroachment, though both increases [*McCulley et al.*, 2004; *Brantley and Young*, 2010] and decreases [*Kieft et al.*, 1998] have been reported. In a cross-site comparison of encroachment-produced shrublands and uninvaded grasslands, *Jackson et al.* [2002] found that woody encroachment resulted in increased soil carbon stocks at sites with low mean annual precipitation (MAP) and decreased soil organic carbon (SOC) stocks at more mesic sites. *Barger et al.* [2011] performed a broader meta analysis and found that, while the relationship between MAP and SOC change with woody encroachment was generally negative, a wide range of outcomes could be observed at a given MAP value. Understanding the mechanisms behind the observed pattern is a challenge because the change in vegetation structure associated with the encroachment of trees and shrubs affects the soil carbon cycle in several ways.

[4] Soil carbon abundance is determined by a mass balance between inputs from primary productivity and losses

---

[1] Department of Civil and Environmental Engineering, Princeton University, Princeton, New Jersey, USA.

Corresponding Author: F. C. O'Donnell, Department of Civil and Environmental Engineering, Engineering Quad E-209A, Princeton University, Princeton, NJ 08544, USA. (fodonnel@princeton.edu)

0148-0227/12/2011JG001899

from decomposition. Shrublands tend to be more productive than grasslands under the same growing conditions [*Norris et al.*, 2001; *Knapp et al.*, 2008], thus woody encroachment can increase input. The effect of vegetation structure on soil carbon decomposition is more complex. Moisture availability, the primary control on biotic decomposition in most dryland ecosystems [*Jenerette et al.*, 2008; *Austin et al.*, 2009], may be lower or higher beneath shrub canopies [*Kieft et al.*, 1998; *Bhark and Small*, 2003; *D'Odorico et al.*, 2007; *Hamerlynck et al.*, 2011]. Canopies exert a local influence on several components of the soil moisture balance, including the direct effects of rainfall interception and reduction of energy for bare soil evaporation. The root systems of plants also reduce soil moisture through root water uptake, but their spatial distribution is less certain. The relative importance of these mechanisms in the soil moisture balance depends on characteristics of the vegetation, as well as the soil type and rainfall climatology [*Rodriguez-Iturbe et al.*, 1999; *Laio et al.*, 2001a]. Inputs to both aboveground and belowground litter pools also occur where canopies and root systems are present, creating spatial correlation between substrate availability and soil moisture conditions that may be more or less favorable for decomposition. Differences in soil carbon abundance between under-canopy and between-canopy patches occur in both grasslands [e.g. *Hook and Burke*, 2000] and shrublands [e.g. *Schlesinger et al.*, 1990; *Wang et al.*, 2009], but shrubs create a more pronounced spatial pattern [*Gonzalez-Polo and Austin*, 2009; *Liu et al.*, 2010]. *Cable et al.* [2012] found that a number of factors, including soil moisture and litter and root abundance, combined to produce significant differences in soil respiration among several microsites, including shrubs, grasses, and open spaces.

[5] Process-based models can provide insight into the mechanisms underlying patterns observed in complex systems by predicting the response of the system to changes in individual parameters. Robust models of soil carbon dynamics exist for water-limited ecosystems [*Porporato et al.*, 2003a], but virtually all soil carbon models assume spatial homogeneity at the scale of vegetation patches [*Manzoni and Porporato*, 2009]. Accurately characterizing the effect of woody encroachment on soil carbon requires a model that can simulate the difference in spatial vegetation structure between a grassland and shrubland. *Hibbard et al.* [2003] used the CENTURY model [*Parton et al.*, 1994] to show how ecosystem carbon pools in a Texas grassland evolved as simulated shrub encroachment occurred. While useful in describing temporal dynamics, the need for a simulation in time and explicit spatial domain makes it difficult to use this approach to evaluate SOC dynamics over a range of ecosystem characteristics.

[6] We present a new model of steady-state dryland soil carbon stocks that uses a probabilistic description of vegetation structure to account for spatial heterogeneity at the patch scale. It is uniquely suited to provide a mechanistic understanding of the effects of woody encroachment on soil carbon stocks, because it is able to simulate the local effects of plant canopies and root systems on both soil carbon inputs and decomposition microenvironment. We parameterize the model for three pairs of shrubland and grassland sites spanning a climate gradient in the western United States and investigate the role of different ecosystem characteristics in producing the observed pattern of SOC change. Our analysis suggests that the spatial structure created by woody encroachment is a key factor leading to changes in soil carbon stocks. Thus, the spatial heterogeneity of both carbon reservoirs and soil moisture dynamics should be accounted for in projections of future carbon budgets for dryland regions.

2. Model Description

[7] The model consists of a system of four coupled differential equations describing the mass balances of soil moisture and three SOC pools. The dynamics of soil moisture and the carbon pools evolve deterministically with perturbations introduced by stochastic rainfall. To address the issue of spatial heterogeneity induced by vegetation structure, we have adapted the approach of *Caylor et al.* [2006] and introduce three variables describing the vegetation structure at a point: n_C, the number of shrub canopies overlapping the point; n_R the number of shrub root systems overlapping the point; and G, which is equal to 1 if the point is covered by a perennial grass patch and equal to 0 otherwise. We assume that grass patches do not overlap, and the "shrubs" in the model could also be trees. The model computes unique results for each combination of n_R, n_C, and G. We take a weighted average of the model results to be indicative of landscape SOC stocks. We assume steady-state conditions to make possible analyses of the effect of patch-scale vegetation structure on SOC and the relative sensitivity of SOC in shrub- and grass-dominated landscapes to vegetation, climate, and soil parameters. *Hibbard et al.* [2003] modeled the transient dynamics of SOC during shrub encroachment and found only monotonic changes. Though many landscapes affected by woody encroachment may not be in steady state, we would expect this to influence the accuracy of the absolute SOC abundance predicted by the model, but not the pattern of relative differences that we are trying to explain. We describe our temporal and spatial averaging methods in sections (2.4) and (2.6).

2.1. SOC Dynamics

[8] Following *Porporato et al.* [2003a], we model SOC as a three-pool system, with coupled differential equations characterizing the dynamics of carbon in fast-decaying litter (C_f), slow-decaying organic matter (C_s), and microbial biomass (C_b) in units of gC m^{-3}, such that

$$\begin{aligned}
\frac{\mathrm{d}C_f}{\mathrm{d}t} &= \frac{\mathrm{ADD}}{Z_r} - \mathrm{DEC}_f + k_b C_b \\
\frac{\mathrm{d}C_s}{\mathrm{d}t} &= r_s \mathrm{DEC}_f - \mathrm{DEC}_s \\
\frac{\mathrm{d}C_b}{\mathrm{d}t} &= (1 - r_r - r_s)\mathrm{DEC}_f + (1 - r_r)\mathrm{DEC}_s - k_b C_b,
\end{aligned} \tag{1}$$

where r_r is the fraction of decomposed organic matter that is lost as CO$_2$ (i.e. $1 - r_r$ is the microbial efficiency), r_s is the fraction of fast-decaying litter that is stabilized by physical and chemical factors that make it less available to decomposers, and k_b is the rate constant for death of microbial biomass (m^{-3} d^{-1}). ADD is the rate of inputs from vegetation (gC m^{-2} d^{-1}), which we discuss in section (2.3), and Z_r is the active soil depth (m).

[9] The decomposition rates of organic matter (DEC$_f$ and DEC$_s$; gC m^{-3} d^{-1}) represent the stochastic component of the equation. We model decomposition of the two substrate pools using first-order rate kinetics with constants k_f and k_s (m^{-3} d^{-1}; $k_f \gg k_s$) that represent the decomposition rates in the absence of water stress. This is a simple approach that works well in cases where a physical factor, soil moisture in this system, is the dominant limitation on decomposition [*Manzoni and Porporato*, 2009]. We calculate the DEC terms as

$$\begin{aligned}\mathrm{DEC}_f &= W[s(t)]k_fC_f\\ \mathrm{DEC}_s &= W[s(t)]k_sC_s,\end{aligned} \tag{2}$$

where $W[s(t)]$ is a dimensionless parameter describing soil moisture limitation of decomposition as a function of relative soil moisture content, $s(t)$ (m^{3}H$_2$O m^{-3} void space). This term represents the stochastic forcing in the SOC system. We incorporate short-term variability in soil moisture into the decomposition term while assuming a constant temperature. Temperature-based respiration models do not perform well in water-limited ecosystems [*Reichstein et al.*, 2003; *Bahn et al.*, 2010], and soil moisture controls the variability of respiration at short time scales [*Xu and Baldocchi*, 2004] due to the necessity of water for both microbial activity and substrate diffusion [*Davidson et al.*, 2006]. We calculate $W[s(t)]$ using the formulation presented by *Cabon et al.* [1991] and *Gusman and Marino* [1999] in which the parameter increases linearly from 0 at a microbial wilting point (s_b) to 1 at field capacity (s_{fc}) and decreases hyperbolically up to soil saturation (s = 1), such that

$$W[s(t)] = \begin{cases} 0, & s \le s_b, \\ \dfrac{s}{s_{fc}}, & s_b < s \le s_{fc} \\ \dfrac{s_{fc}}{s}, & s_{fc} < s \le 1. \end{cases} \tag{3}$$

[10] We determine s with a model of soil moisture dynamics forced by stochastic rainfall, as described in the following section.

2.2. Soil Moisture Dynamics

[11] *Rodriguez-Iturbe et al.* [1999] and *Laio et al.* [2001a] model the daily soil moisture balance of the plant rooting zone with the stochastic differential equation

$$nZ_r\frac{\mathrm{d}s(t)}{\mathrm{d}t} = R(t) - I(t) - Q[s(t);t] - ET[s(t)] - L[s(t)], \tag{4}$$

where n is the soil porosity, Z_r is the depth of the active root zone, and $s(t)$ is the relative soil moisture content. Inputs of water from stochastic rainfall [$R(t)$] are modeled as a marked Poisson process of storms with arrival rate λ_r (d^{-1}) and exponentially distributed depth with mean α (mm). Inputs are balanced by losses due to canopy interception [$I(t)$], runoff ($Q[s(t);\ t]$), evapotranspiration ($ET[s(t)]$), and drainage ($L[s(t)]$).

[12] *Caylor et al.* [2006] extend the probabilistic soil moisture modeling framework to heterogeneous landscapes by parameterizing equation (4) for each combination of n_C and n_R to account for the local effects of shrub canopies and root systems on the soil moisture balance. We modify this approach to include grass. We characterize the influence of the structural differences between grasses and shrubs on aboveground processes but are unable to account for potential differences in rooting depth between shrubs and grasses within the modeling framework. When averaged globally, shrublands have deeper roots than grasslands [*Jackson et al.*, 1996]. However, there is mixed evidence on whether shrubs and grasses growing in the same conditions have different rooting depths [*Schenk and Jackson*, 2002], especially in the case of fine roots [*Bai et al.*, 2009], which produce most below ground contributions to labile carbon pools. Additionally, the majority of water uptake by woody plants is from surface layers [*Kulmatiski et al.*, 2010]. Since soil moisture and SOC input are the processes of interest in this study, we assume equal active soil depths for grasses and shrubs.

[13] At points covered by grass and shrub canopies, some rainfall will be intercepted by and evaporated directly from plant canopies without reaching the soil. The depth of rainfall reaching the soil in a given storm is the storm depth minus a characteristic interception value, $\Delta(n_C, G)$ (mm), or 0 if the storm depth is less than $\Delta(n_C, G)$. We estimate Δ empirically as

$$\Delta(n_C, G) = LAI_s \times h \times n_C + LAI_g \times h \times G, \tag{5}$$

where LAI_s and LAI_g are the leaf area index (LAI; m^2 m^{-2}) beneath a single shrub canopy and a typical grass patch, respectively. The parameter h is the characteristic amount of interception per unit leaf area, which we take to be 1 mm [*Aston*, 1979]. If the depth of non-intercepted rainfall exceeds available storage in the soil, the excess is converted to surface run-off ($Q[s(t);\ t]$).

[14] Once water has infiltrated the soil, it leaves via drainage and evapotranspiration, which constitute the soil moisture-dependent loss function of the system. Following *Laio et al.* [2001a], we model the rate of gravity-driven drainage as an exponential decay from the saturated hydraulic conductivity of the soil (K_s; mm d^{-1}) at s = 1 to 0 at soil field capacity, independent of n_C, n_R, and G. Plants reduce bare soil evaporation by shading and determine the spatial distribution of water loss via root uptake, so we model the evaporation and transpiration components separately, following *Caylor et al.* [2006]. The interception of energy and loss of water through leaves, which we will refer to as transpiration, may be spatially decoupled from the absorption of soil moisture by roots, which we will refer to as uptake. In the original model formulation, potential evapotranspiration (PET; mm d^{-1}) provided an upper bound on the rate of soil moisture loss via evapotranspiration. To provide upper bounds on the processes of shrub transpiration, grass transpiration, and bare soil evaporation we multiply PET, which we take to be a constant, long-term value, by the fractions of incoming energy absorbed by shrub canopies, grass canopies, and the soil surface. We model canopy energy interception using Beer's law and assume shrub canopies are taller than grass canopies. Thus, the fractions of incident radiation at a point contributing to

potential shrub transpiration (Φ_s), grass transpiration (Φ_g), and evaporation (Φ_E) are given by

$$\begin{aligned} \Phi_s &= e^{-kLAI_s n_C} \\ \Phi_g &= [1 - \Phi_s] e^{-kLAI_g G} \\ \Phi_e &= 1 - \Phi_s - \Phi_g, \end{aligned} \tag{6}$$

where k is the extinction coefficient of evaporative demand, which we take to be 0.35 [*Brutsaert*, 1982]. We calculate these terms recursively to represent the vertical structure of the ecosystem.

[15] Evaporation and uptake by grasses, which we assume do not have roots extending beyond their canopies, extract water from areas of soil directly below the surfaces absorbing the energy that drives these processes. Therefore, the maximum rates of soil moisture loss from evaporation and grass uptake (φ_e and φ_g; mm d^{-1}) at a point are a function of the energy interception pattern at that point:

$$\begin{aligned} \varphi_e(n_C, G) &= \Phi_e(n_C, G) \times PET \\ \varphi_g(n_C, G) &= \Phi_g(n_C, G) \times PET. \end{aligned} \tag{7}$$

The root system of a shrub may extend well beyond its canopy edge, so shrubs can extract water from the soil at points not overlapped by their canopies. By doing this, shrubs spatially decouple transpiration and uptake. In some landscapes grasses also have laterally extensive root systems [*Casper et al.*, 2003], in which case the formulations for the belowground structure and function of shrub roots could be applied to grasses. To estimate the maximum rate of uptake by shrubs for a point with n_R overlapping shrub root systems, it is necessary to estimate the energy absorbed by the canopy associated with each root system. Some canopies will absorb less energy per unit area because they overlap with others, but it would be computationally intensive to model them individually. We simplify the system by calculating the fraction of incident energy absorbed by a shrub canopy with an average amount of overlap with other canopies, $\overline{\Phi_s}$, following [*Caylor et al.*, 2006]. This is given by the summation of the fraction of energy absorbed by a canopy at a point with each n_C value, weighted by the fraction of the canopy-covered landscape ($n_C \geq 1$) with that n_C value, such that

$$\overline{\Phi_s} = \sum_{n_C=1}^{\infty} \left(\frac{1 - e^{-kn_C}}{n_C} \right) \frac{P_{n_C}(n_C)}{1 - P_{n_C}(0)}, \tag{8}$$

where $P_{n_C}(n_C)$ is the probability that a point on the landscape is overlapped by n_C canopies. Its derivation is described in section (2.5). We update an earlier form of the model [*Caylor et al.*, 2006] by multiplying $\overline{\Phi_s}$ by the ratio of the average canopy area (A_C, m^2) to the average root system area (A_R, m^2), because energy absorbed by the canopy drives uptake through the entire root system. This results in a lower estimate of potential uptake at a point. The potential shrub uptake at a point (mm d^{-1}) is given by

$$\varphi_s(n_R) = n_R \times \frac{A_C}{A_R} \times \overline{\Phi_s} \times PET. \tag{9}$$

[16] Evaporation and uptake may also be limited by soil moisture. The bare soil evaporation rate ranges from zero at the soil hygroscopic point to its maximum rate (φ_e) at the soil field capacity and above. We model the rate with a linear increase between these two points (following *Caylor et al.* [2006]). We model uptake with a similar linear model ranging from zero at the plant wilting point, s_w, to a maximum at the point of incipient stomatal closure, s^* [following *Laio et al.*, 2001a]. This leads to a unique soil moisture loss function for each combination of n_C, n_R, and G.

2.3. Productivity and SOC Input

[17] The SOC model also requires that vegetation productivity be estimated so the addition term, ADD (gC m^{-2} d^{-1}), can be determined. Water is the primary limitation on photosynthesis in the ecosystems considered in this study, so we model carbon assimilation as the product of transpiration (mm) occurring over the course of a day and measured water use efficiency values (gC mm^{-1} H_2O; measured values from *Scholes and Walker* [1993]). In doing this, we assume that water use efficiency does not decrease when plants are under water stress. However, this simplifying assumption could easily be removed if information on the relationship between water use efficiency and soil moisture were available. We calculate grass and shrub net primary productivity (NPP) separately, such that

$$\begin{aligned} NPP_g &= WUE_g \times T_g[s(t)] \\ NPP_s &= WUE_s \times T_s[s(t)], \end{aligned} \tag{10}$$

where WUE_g and WUE_s are the water use efficiency values for grasses and shrubs. Measured values of NPP_g and NPP_s could be substituted if available. Growth and mortality create a time lag between transpiration and SOC input. We assume that these processes are in equilibrium, so SOC input rate can be modeled using the equations in (10). This assumption allows us to derive a steady-state solution to the SOC model, which we describe in section (2.4). We present a comparison of our simple empirical representation of productivity with more complex, mechanistic physiology models in Appendix B. The simple model captures the trend of increasing productivity with increasing rainfall and vegetation density, while allowing us to develop a tractable model that accounts for patch-scale vegetation heterogeneity.

[18] One of our goals is to account for the local effects of vegetation patches on both inputs to and decomposition of SOC. Therefore, it is necessary to calculate ADD, the SOC addition rate defined in equation (1), as a function of n_C, n_R, and G. Grasses and shrubs affect the SOC input rate differently, so we introduce separate addition terms that sum to ADD. The aboveground and belowground biomass of grasses contributes to SOC over the same area, but shrub root systems and canopies, which respectively determine the spatial distribution of inputs from belowground and aboveground biomass cover different areas. Therefore, it is necessary to divide NPP_s into aboveground and belowground components. We make the simplifying assumption that aboveground/belowground plant allocation is proportional to the ratio of average canopy area to average root system area, so the fraction of biomass allocated aboveground is equal to A_C/A_R.

[19] We then determine the addition term at a point by multiplying NPP_g and NPP_s by vegetation structure weighting terms, which are a function of n_C, n_R, and G:

$$\mathrm{ADD} = \vartheta_g(G) \times NPP_g + \vartheta_s(n_C, n_R) \times NPP_s. \tag{11}$$

The vegetation structure weighting terms are determined by dividing n_C, n_R, and G by their expected values, such that

$$\vartheta_g(G) = \frac{G}{\mathrm{E}[G]} \tag{12}$$

for grasses and

$$\vartheta_s(n_C, n_R) = \frac{n_C}{\mathrm{E}[n_C]}\left(\frac{A_C}{A_R}\right) + \frac{n_R}{\mathrm{E}[n_R]}\left(1 - \frac{A_C}{A_R}\right) \tag{13}$$

for shrubs. Expected values are denoted by the operator $\mathrm{E}[\cdot]$ and are derived from the probability distributions of n_C, n_R, and G, which we define in section (2.6).

[20] Abiotic processes, primarily photodegradation, have been identified as having significant effects on surface litter dynamics in dryland ecosystems [*Austin and Vivanco*, 2006; *Rutledge et al.*, 2010]. A term could be added to reduce the addition rate to account for this. We did not do so, because reported rates of mass loss from photodegradation are less than 16 g m^{-2} yr^{-1} [*Austin*, 2011], which is small compared to NPP and thus unlikely to significantly reduce soil carbon inputs.

2.4. Temporal Averaging

[21] The SOC model given by equation (1) represents a system that exhibits deterministic behavior with perturbations driven by stochastic rainfall, as described in section 2.1. Previous stochastic models of hydrologically-driven soil biogeochemistry have relied on a rainfall simulation to force the model [*Porporato et al.*, 2003a; *Wang et al.*, 2009]. The simulation approach, which models soil moisture dynamics with a daily time step, is useful in drylands, where decomposition rates respond quickly to rainfall events [*Xu and Baldocchi*, 2004; *Jarvis et al.*, 2007]. Such a model is impractical in our case, because unique simulations would need to be run for each combination of n_C, n_R, and G. To address this, we introduce a steady-state version of the SOC model. For simplicity, we describe the three state variables in the SOC system, fast-decaying litter (C_f), stabilized organic matter (C_s), and microbial biomass (C_b), as a vector:

$$\mathbf{x}_t = \begin{bmatrix} C_f(t) \\ C_s(t) \\ C_b(t) \end{bmatrix}. \tag{14}$$

The temporal dynamics of the SOC pools, driven by stochastic soil moisture, for a given combination of n_C, n_R, and G can be described as a function of $\mathbf{x}_t$. It is derived from equation (1) by substituting the expressions relating decomposition rates (DEC_f and DEC_s) and SOC input rate (ADD) to soil moisture, which are described by equations (3) and (11), respectively, giving

$$\frac{\mathrm{d}\mathbf{x}_t}{\mathrm{d}t} = \begin{bmatrix} \vartheta_g WUE_g T_g[s(t)] + \vartheta_s WUE_s T_s[s(t)] - W[s(t)] k_f C_f + k_b C_b \\ r_s W[s(t)] k_f C_f - W[s(t)] k_s C_s \\ (1 - r_s - r_r) W[s(t)] k_f C_f + (1 - r_r) W[s(t)] k_s C_s - k_b C_b \end{bmatrix}. \tag{15}$$

The terms relating transpiration ($T_g[s(t)]$ and $T_s[s(t)]$) and decomposition rate ($W[s(t)]$) to soil moisture control the variability of $\mathbf{x}_t$ in time.

[22] We simplify equation (15) by dividing it into two components: (1) a deterministic expression, given by $\mathbf{H}(\mathbf{x}_t)$, describing the behavior of the system under average conditions, and (2) an expression, given by $\mathbf{h}(\mathbf{x}_t)$, describing the variability introduced to the system by the stochastic nature of soil moisture. The deterministic component is given by evaluating $\mathrm{d}\mathbf{x}_t/\mathrm{d}t$ for temporal averages of $T_g[s(t)]$, $T_s[s(t)]$, and $W[s(t)]$:

$$\mathbf{H}(\mathbf{x}) = \begin{bmatrix} \varphi_g \mathrm{WUE}_g \langle T_g[s(t)] \rangle + \varphi_s \mathrm{WUE}_s \langle T_s[s(t)] \rangle - \langle W[s(t)] \rangle k_f C_f + k_b C_b \\ r_s \langle W[s(t)] \rangle k_f C_f - \langle W[s(t)] \rangle k_s C_s \\ (1 - r_s - r_r) \langle W[s(t)] \rangle k_f C_f + (1 - r_r) \langle W[s(t)] \rangle k_s C_s - k_b C_b \end{bmatrix}, \tag{16}$$

where $\langle \cdot \rangle$ indicates a temporal average. To determine the temporal averages in equation (16), we follow the approach presented by *Rodriguez-Iturbe et al.* [1999] and *Laio et al.* [2001a] and modified by *Caylor et al.* [2006]. We solve the stochastic differential equation describing the soil moisture balance (equation (4)) for the steady-state probability density function of soil moisture in time, $p_S(s)$, for each combination of n_C, n_R, and G. The temporal averages of transpiration rate and the decomposition limitation term are given by their expected values:

$$\langle X[s(t)] \rangle = \int_0^1 X(u) p_S(u) \mathrm{d}u, \quad X = W, T_s, T_g. \tag{17}$$

[23] The deterministic system described by equation (16) is an adequate representation of soil carbon additions, because growth and mortality decouple this process from the temporal variability of soil moisture. However, it is important to account for the influence of soil moisture variability on decomposition rate through the limitation term $W[s(t)]$. To do so, we first define the system $\mathbf{h}(\mathbf{x}_t)$ as all components of equation (15) that multiply $W[s(t)]$:

$$\mathbf{h}(\mathbf{x}) = \begin{bmatrix} -k_f C_f \\ r_s k_f C_f - k_s C_s \\ (1 - r_s - r_r) k_f C_f + (1 - r_r) k_s C_s \end{bmatrix}. \tag{18}$$

We then approximate $W[s(t)]$ as the sum of its temporal average and zero-mean, normally distributed perturbations (white noise), such that

$$W[s(t)] \approx \langle W[s(t)] \rangle + \xi \sqrt{\sigma_W^2}, \tag{19}$$

where ξ is a normally distributed random variable with mean 0 and variance 1, and σ_W^2 is the variance of $W[s(t)]$. This approximation of the variability of decomposition conditions as white noise assumes no temporal autocorrelation in the values of $W[s(t)]$, which is physically unrealistic. However, other applications of multiplicative noise models in environmental systems have made the same assumption about temporally autocorrelated variables such as wind speed [*Brubaker and Entekhabi*, 1996] and precipitation [*Rodriguez-Iturbe et al.*, 1991] without introducing significant model error. We present a comparison of our model results with a simulation-based form that does not make this assumption in Appendix A.

[24] The variance of $W[s(t)]$ in equation (19) is given by

$$\sigma_W^2 = \mathrm{E}[W[s(t)]^2] - \mathrm{E}[W[s(t)]]^2. \tag{20}$$

The expected value of $W[s(t)]$ is its temporal average, given by equation (17). Following the approach used in equation (17), we derive the expected value of $W[s(t)]^2$ using the probability density function of s, so that the full expression for the variance of $W[s(t)]$ is

$$\sigma_W^2 = \int_0^1 W(u)^2 p_S(u)\mathrm{d}u - \langle W[s(t)]\rangle^2. \tag{21}$$

[25] Combining the deterministic and stochastic components leads to a single expression describing the dynamics of the system:

$$\mathrm{d}\mathbf{x}_t = \mathbf{H}(\mathbf{x}_t)\mathrm{d}s + \sigma_W \mathbf{h}(\mathbf{x}_t)\mathrm{d}w_t, \tag{22}$$

where $\mathrm{d}w_t$ is the infinitesimal of a Wiener process. We then solve equation (22) numerically to determine the steady-state sizes of the SOC pools for a point on the landscape covered by a given combination of n_C, n_R, and G. In our analysis of the interactions between vegetation structure, soil moisture, and soil carbon, it is useful to determine temporal averages of all components of the soil moisture balance as a function of n_C, n_R, and G. The temporal means (mm d^{-1}) of the soil moisture-dependant processes of leakage, evaporation, and transpiration are calculated in the same way as mean soil moisture, as described in equation (17). We calculate the average daily canopy interception following *Laio*, *et al.* [2001a]:

$$\langle I(n_C, G)\rangle = \alpha\lambda_r\left(1 - \exp\left[-\frac{\Delta(n_C, G)}{\alpha}\right]\right). \tag{23}$$

In the following sections, we describe the spatial averaging methods used to determine landscape averages of the SOC pools and components of the soil moisture balance.

2.5. Vegetation Structure

[26] Following the approach presented by *Caylor et al.* [2006], we use a probabilistic description of vegetation structure based on a two-dimensional, marked Poisson point process. Using a random point process neglects any clustering or inhibition in the location of shrubs but enables us to determine analytically the fraction of the landscape covered by each combination of n_C, n_R, and G. We model shrub locations as a Poisson process of rate λ_s (individuals m^{-2}) with circular canopies having radii drawn from an exponential distribution of mean μ_s (m). We assign the ratio of root radius to canopy radius of an individual, a_t, a constant value of 2, following *Caylor et al.* [2006]. Because we assume this description of shrub location and size, the probability that a point on the landscape is covered by a number of root systems, n_R, is given by a Poisson distribution

$$P_{n_R}(n_R) = \frac{(2\lambda_s\pi\mu_r^2 a_t^2)^{n_R} e^{-2\lambda_s\pi\mu_r^2 a_t^2}}{n_R!}(n_R = 0, 1, \ldots) \tag{24}$$

where 0! is, by definition, equal to 1. The probability that a point is overlapped by a number of canopies, n_C, is given by

$$P_{n_C}(n_C) = \frac{(2\lambda_s\pi\mu_r^2)^{n_C} e^{-2\lambda_s\pi\mu_r^2}}{n_C!}(n_C = 0, 1, \ldots). \tag{25}$$

Because canopies and root systems are connected, n_C and n_R are not independent. We address this by calculating the conditional probability that a point overlapped by n_R root systems is overlapped by a number of canopies, n_C, given by

$$P_{n_C|n_R}(n_C|n_R) = \binom{n_R}{n_C}\left(\frac{1}{a_t^2}\right)^{n_C}\left(1 - \frac{1}{a_t^2}\right)^{n_R}(n_C = 0, 1, \ldots, n_R). \tag{26}$$

Equations (24) and (26) can be used to find the joint distribution of n_R and n_C and the expected fraction of the landscape covered by any combination of n_R and n_C values such that $n_R \geq n_C$.

[27] We consider the shading effects of shrub canopies when calculating the probability that G is equal to one for a point, because grass productivity has been shown to be inversely related to shrub LAI in mixed shrub-grass systems [*Caylor et al.*, 2004]. As with our calculation of canopy energy interception, we estimate shading effects using Beer's law. G is determined so that its expected value equals measured grass fractional cover, c_g. We calculate the probability that $G = 1$ for a point overlapped by n_C canopies as

$$P_{G|n_C}(1|n_C) = c_g e^{-kn_C}\left[\sum_{i=0}^{\infty} e^{-ik} P_{n_C}(i)\right]^{-1}. \tag{27}$$

Note that the term in brackets is the expected value of e^{-kn_C} on the landscape.

2.6. Spatial Averaging

[28] As outlined in section (2.4), we calculate unique, steady state values of the SOC pools ($\langle C_f(n_C, n_R, G)\rangle$, $\langle C_s(n_C, n_R, G)\rangle$, and $\langle C_b(n_C, n_R, G)\rangle$) and components of the soil moisture balance ($\langle I(n_C, G)\rangle$, $\langle E(n_C, n_R, G)\rangle$, $\langle T_g(n_C, n_R, G)\rangle$, $\langle T_s(n_C, n_R, G)\rangle$, and $\langle L(n_C, n_R, G)\rangle$) for each combination of n_C, n_R, and G. To find a landscape average of any of these values, we take an average over the combinations of n_C, n_R, and G values weighted by the fraction of the landscape covered by each combination. Utilizing the conditional probability distributions presented in the previous section, this is given by

$$\begin{aligned}\overline{\langle X\rangle} = \sum_{n_R=0}^{\infty}&\Big[P_{n_R}(n_R)\sum_{n_C=0}^{n_R} P_{n_C|n_R}(n_C|n_R)\\ &\times\left(\langle X(n_C, n_R, 1)\rangle P_{G|n_C}(1|n_C) + \langle X(n_C, n_R, 0)\rangle P_{G|n_C}(0|n_C)\right)\Big]\\ &(X = C_f, C_s, C_b, I, E, T_g, T_s, L),\end{aligned} \tag{28}$$

where the overbar indicates a spatial average.

[29] The turnover time for the stabilized organic matter pool is usually larger than the timescales on which changes in vegetation structure occur. Therefore, if we wish to calculate the total SOC abundance for a point on the landscape,

Table 1. General Model Parameters

Parameter	Symbol	Value	Source
Soil hygroscopic point[a]	Ψ_h	-10 MPa	*Laio et al.* [2001a]
Microbial wilting point[a]	Ψ_b	-6 MPa	*Porporato et al.* [2003a]
Vegetation wilting point[a]	Ψ_w	-5 MPa	*Laio et al.* [2001a]
Point of incipient stress[a]	Ψ^*	-0.03 MPa	*Laio et al.* [2001a]
Active soil depth	Z_r	1[b] m	*Jackson et al.* [2002]
Characteristic canopy interception	h	1 mm/unit LAI	*Scholes and Walker* [1993]
Extinction coefficient of evaporative demand	k	0.35	*Brutsaert* [1982]
Shrub water-use efficiency	WUE_s	3.6×10^{-3} gC gH$_2$O^{-1}	*Scholes and Walker* [1993]
Grass water-use efficiency	WUE_g	5.0×10^{-3} gC gH$_2$O^{-1}	*Scholes and Walker* [1993]
Root system to canopy radius ratio	a_t	2	*Caylor et al.* [2006]
C_f decay constant	k_f	[c]6.5×10^{-3} m^3 d^{-1}	*D'Odorico et al.* [2003]
C_s decay constant	k_s	[c]2.5×10^{-4} m^3 d^{-1}	*D'Odorico et al.* [2003]
Microbial death rate	k_b	8.5×10^{-3} d^{-1}	*D'Odorico et al.* [2003]
Isohumic coefficient	r_s	0.25	*D'Odorico et al.* [2003]
Microbial efficiency	r_r	0.4	*D'Odorico et al.* [2003]

[a] Converted to relative soil moisture (s) values using soil texture-specific relationships from *Clapp and Hornberger* [1978].

[b] Average 95% rooting depth for study sites.

[c] Based on an average microbial biomass abundance of 100 gC m^{-3}.

we add point-specific values for C_f and C_b to the landscape average of C_s abundance, such that

$$\mathbf{C}(n_C, n_R, G) = Z_r \times \left[\overline{\langle C_s \rangle} + \langle C_f(n_C, n_R, G) \rangle + \langle C_b(n_C, n_R, G) \rangle\right] \tag{29}$$

where we multiply by the active soil depth, Z_r, to express $\mathbf{C}$ in units of gC m^{-2}. As with the individual pools, we determine a weighted landscape average of SOC abundance for intersite comparisons, which is given by

$$\overline{\mathbf{C}} = Z_r \times \left[\overline{\langle C_f \rangle} + \overline{\langle C_s \rangle} + \overline{\langle C_b \rangle}\right]. \tag{30}$$

3. Results

3.1. Model Verification and Application

[30] We tested the ability of the model to replicate SOC dynamics in mixed woody plant-grass ecosystems using data from a series of research sites spanning a climate gradient in Southern Africa. Data on SOC abundance are available for these sites, along with the vegetation structure data necessary to determine the model parameters. The model produced reasonable SOC abundance values for a variety of vegetation types (Appendix B).

[31] To investigate the mechanisms behind SOC loss or accrual following woody encroachment, we parameterized the model for data from three sites in the American Southwest collected by *Jackson et al.* [2002]. The data were presented as part of a six-site analysis of the effect of woody encroachment on SOC stocks along a gradient in MAP. We selected three sites for which the vegetation structure data necessary to determine model parameters was available in the literature. The driest site, Jornada, New Mexico, is a desert grassland dominated by *Bouteloua eriopoda* (black grama) and subject to invasion by *Larrea tridentata* (creosote bush), which has been associated with an increase in near-surface (0–1 m depth) SOC stocks. At the semi-arid Central Plains Experimental Range (CPER) in Colorado, *Atriplex canescens* (saltbush) invasion of *Bouteloua gracilis* (blue grama) steppe led to a decrease in SOC stocks. An even larger decrease in SOC stocks was observed at the most mesic of the three sites, Riesel, Texas, where *Schizachyrium scoparium* (little bluestem)-dominated tallgrass prairie is invaded by *Prosopis glandulosa* (honey mesquite). These three sites span the precipitation gradient, with mean annual totals of 270, 322, and 840 mm, respectively. For each site, we parameterized the model for two communities, one an uninvaded grassland and one a shrubland produced by encroachment at least 30 years prior to SOC measurements. General and site-specific model parameters are given in Tables 1 and 2.

[32] A comparison of the model results with data from *Jackson et al.* [2002] is shown in Table 3. The model successfully replicated the general pattern of increasing SOC storage for all ecosystems with increasing MAP, and of shrublands storing more SOC in the most arid regions and grasslands storing more SOC at sites with higher MAP, as shown in Figure 1. In the following sections, we use our modeling approach to examine the mechanisms behind the observed pattern.

3.2. SOC, Climate, and Vegetation Couplings

[33] Determining the mechanisms driving the pattern of SOC change observed along a precipitation gradient is a challenge because a number of factors influencing productivity and decomposition are related to MAP. Our modeling approach makes it possible to isolate these factors and their influence on SOC stocks. The sites analyzed also have increasingly fine soil texture with higher precipitation. Increasing rainfall or changing soil texture while holding the other parameters constant did not produce a shift towards grass-dominated systems storing more SOC (see analysis in Appendix C). Thus, the indirect effects of climate and soil texture on vegetation structure are more important in determining the effect of woody encroachment on SOC stocks.

[34] The sites differ greatly in abundance and structure of vegetation. The fractional vegetation cover, equal to the grass fractional cover (c_g) for grasslands and the sum of woody and grass fractional cover for shrublands ($c_s + c_g$; Table 2), increases along the climate gradient but was largely unchanged by shrub encroachment at the individual sites. Additionally, the LAI of individual shrub canopies and grass patches (LAI_s and LAI_g) both increase along the

Table 2. Site-Specific Model Parameters

Parameter	Symbol	Units	Jornada, NM		CPER, CO		Riesel, TX	
Soil texture	-	-	Loamy sand[a]		Sandy clay loam[b]		Clay loam[c]	
Mean storm depth	α	mm	5.2[d]		5.3[d]		10[e]	
Storm frequency	λ_r	d^{-1}	0.25[d]		0.30[d]		0.28[e]	
Potential evapotranspiration	PET	mm d^{-1}	4.3[f]		3.7[g]		4.8[e]	
Shrub canopy LAI	LAI_s	$m^2\ m^{-2}$	1.5[h]		2.0[i]		3.0[j]	
Grass patch LAI	LAI_g	$m^2\ m^{-2}$	0.5[h]		1.0[k]		2.0[j]	
Community Type			Grass	Shrub	Grass	Shrub	Grass	Shrub
Mean canopy radius	μ_s	m	-	0.62[h]	-	1.2[l]	-	1.7[m]
Shrub frequency	λ_s	ind m^{-2}	-	0.14[n]	-	0.036[n]	-	0.049[n]
Woody fractional cover	c_s	-	-	0.29[h]	-	0.28[o]	-	0.59[m]
Grass fractional cover	c_g	-	0.33[h]	0.04[h]	0.59[b]	0.29[o]	0.95[p]	0.37[m]
Landscape LAI	LAI	$m^2\ m^{-2}$	0.16[q]	0.53[q]	0.59[q]	0.94[q]	1.9[q]	3.4[q]

[a] *Howes and Abrahams* [2003].
[b] *Hooke and Burke* [2000].
[c] *Harmel et al.* [2006].
[d] Climate and Hydrology Database Project.
[e] USDA Agricultural Research Service.
[f] *Knapp et al.* [2008].
[g] *Laio et al.* [2001b].
[h] *Gibbens et al.* [1996].
[i] *Glenn et al.* [2008].
[j] *Savabi et al.* [1989].
[k] *Hazlett* [1992].
[l] *Petersen and Ueckert* [2005].
[m] *Ansley et al.* [2001].
[n] Calculated using the relationship $c_s = 1 - \exp(-2\pi\lambda_s\mu_s^2)$.
[o] *Bestelmeyer and Wiens* [2001].
[p] *Derner and Wu* [2004].
[q] Calculated using the relationship $LAI = E[G] \times LAI_g + E[n_C] \times LAI_s$.

gradient, but LAI_g, which goes from 0.5 to 2 $m^2\ m^{-2}$ between Jornada and Riesel, increases by a larger proportion than LAI_s, which goes from 1.5 to 3 $m^2\ m^{-2}$.

[35] To investigate the relationship between vegetation cover and relative SOC abundance, we compared a grass-only with a shrub-only version of the model. We ran the two models over a range fractional covers, setting the parameter equal to grass fractional cover (c_g) for the grass-only model and woody fractional cover (c_s) for the shrub-only model (Figure 2). We did this once using soil, climate, and vegetation parameters (other than vegetation cover) for Jornada and once for Riesel. Changing fractional cover replicated the pattern observed in the measured data only slightly for the landscapes parameterized for Jornada, but markedly for the Riesel landscapes. A high vegetation density appears to be necessary for grasslands to store more SOC than shrublands, but it is clear that other conditions must be met.

[36] We performed a similar analysis holding fractional cover constant at the site-specific values, but varying the LAI of a single shrub canopy and the LAI of a grass patch between the values observed at Jornada and Riesel (Figure 3). Moving from low to high values for both LAI parameters, LAI_g increases relative to LAI_s. Again, the model produced the observed pattern of relative shrubland-grassland SOC abundance, but the change was more pronounced for the Riesel sites. This suggests that both vegetation cover

Table 3. Comparison of Measured and Modeled Steady-State Soil Organic Carbon (SOC) Abundance

		Grassland SOC (MgC ha^{-1})		Shrubland SOC (MgC ha^{-1})	
Site	MAP[a] (mm)	Measured[b]	Modeled	Measured[b]	Modeled
Jornada, NM	230	24.6	19.4	32.9	33.9
CPER, CO	322	89.3	43.6	70.8	41.9
Riesel, TX	840	229	168	164	146

[a] MAP, Mean Annual Precipitation.
[b] Measured values from *Jackson et al.* [2002].

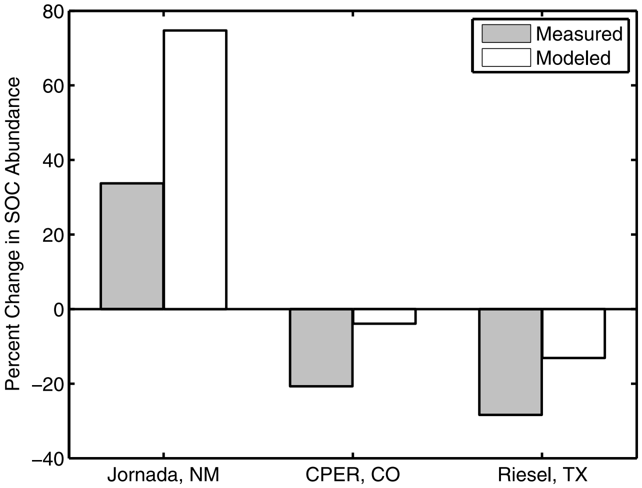

Figure 1. Comparison of modeled and measured percent difference between SOC stocks in paired grassland and shrubland communities at three sites in the American Southwest. White bars show model results with general parameters from Table 1 and site-specific parameters from Table 2. Gray bars show measured values for the top meter of soil from *Jackson et al.* [2002].

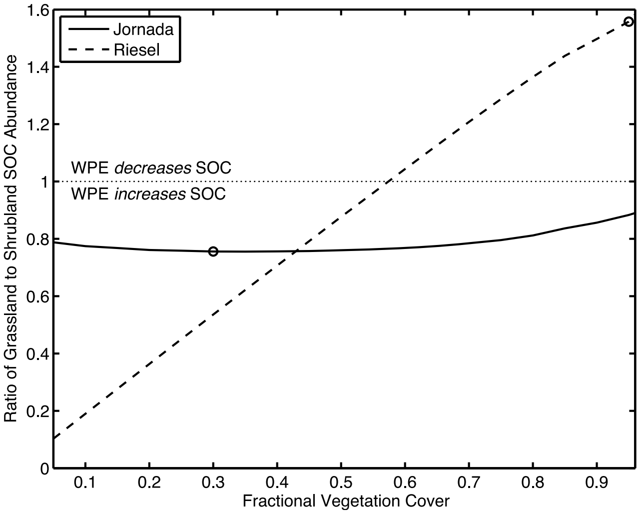

Figure 2. Modeled ratio of SOC stocks in paired landscapes containing only grasses or only shrubs across a range of vegetation densities. Other model parameters for Jornada, NM (black line), and Riesel, TX (dashed line), were used (Table 2). Grassland fractional cover is varied by changing grass percent cover. Shrubland fractional cover is varied by increasing or decreasing mean canopy radius (μ_s). The open circles show the observed vegetation densities at the two sites. Grassland to shrubland SOC ratio may vary from results in Table 3 and Figure 1, which model the shrubland as a mixed shrub-grass community. General model parameters are taken from Table 1.

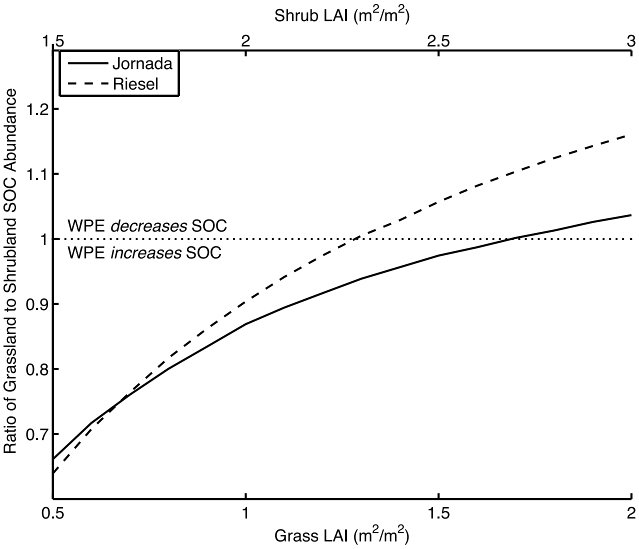

Figure 3. Modeled ratio of SOC stocks in paired landscapes containing only grasses or shrubs across a range of shrub canopy and grass patch leaf area index values. Leaf area index values were increased linearly from the minimum to maximum observed values. Other model parameters for Jornada, NM (black line), and Riesel, TX (dashed line), were used (Table 2). General model parameters are given in Table 1.

and LAI are important in determining which type of landscape will store more SOC at a given site. The vegetation structure characteristics identified as drivers of the pattern of SOC abundance influence multiple components of the soil moisture balance and SOC cycle, which we will examine in the following sections.

3.3. Vegetation Structure and Productivity

[37] The fractional cover and LAI of the vegetation in a landscape are key determinants of transpiration rates and thus productivity. The relative contribution of transpiration to the soil moisture balance of grasslands and shrublands at the three study sites is shown in Figure 4, which compares the temporal and spatial averages of the soil moisture balance components (derived in equation (27)). Landscape average transpiration of the shrubland is around twice that of the grassland at Jornada. While transpiration for the two landscape types is similar at the more mesic sites, grassland transpiration does not surpass the shrubland at Riesel, as might be expected.

[38] Shrubs, with roots extending beyond the canopy, spatially decouple the processes of root water uptake and leaf-level transpiration to a much greater extent than grasses. This has a different effect on sparsely- and densely-vegetated landscapes. Table 4 describes root uptake and distribution in grass- and shrub-dominated landscapes at the three sites. At points on the landscape where roots are present (i.e. $n_R \geq 1$ and/or $G = 1$), the soil moisture uptake of grasses and shrubs is similar. While shrub canopies have a higher LAI and intercept more energy at a point, the energy absorbed must drive uptake over a larger root system area. The laterally-extensive root systems of shrubs cover a much higher fraction of the sparse landscape at Jornada, resulting in higher landscape-level uptake. However, as total vegetation cover increases, landscape-level uptake of grasslands and shrublands converges.

[39] It is difficult to separate the effects of vegetation density and LAI from the study site model results. To address this, we modeled the ratio of landscape average uptake rates for paired landscapes of only shrubs and only grasses, using intermediate

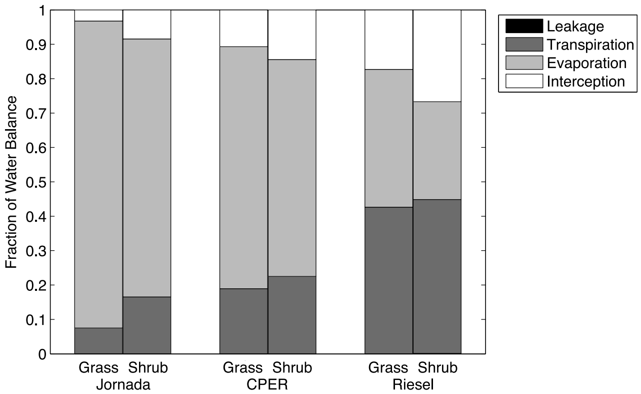

Figure 4. Contribution of leakage (black bars), transpiration (dark gray bars), evaporation (light gray bars), and canopy interception (white bars) to the temporally- and spatially-averaged soil water balance of grass- and shrub-dominated landscapes at three sites in the American Southwest.

Table 4. Modeled Root Uptake and Abundance for Grasslands (G), Shrublands (S), and the Ratio of Grassland to Shrubland Values (G:S) at the Three Study Sites

	Site								
	Jordana			CPER			Riesel		
	G	S	G:S	G	S	G:S	G	S	G:S
Average uptake in root-occupied soil (mm d^{-1})	0.28	0.29	0.97	0.49	0.43	1.13	1.3	1.3	0.99
Fraction of soil occupied by roots	0.33	0.75	0.44	0.59	0.82	0.72	0.95	0.99	0.96
Landscape average uptake (mm d^{-1})	0.09	0.21	0.43	0.29	0.36	0.80	1.2	1.3	0.95

values for the other model parameters (Figure 5). For a given fractional cover, which is closely related to precipitation, a range of uptake ratios is possible based on the relative LAI of the grass and shrub species.

[40] Despite having lower transpiration, the grasslands at CPER and Riesel are more productive than paired shrublands because of the higher water use efficiency of grass (5.0×10^{-3} gC gH_2O^{-1}) relative to shrubs (3.6×10^{-3} gC gH_2O^{-1}). The difference in productivity does not translate directly to differences in SOC storage, because vegetation structure also affects decomposition, which we discuss in the next section.

3.4. Spatially Variable Decomposition

[41] Vegetation structure is important in determining the productivity of a semi-arid ecosystem, but it also influences the decomposition side of SOC dynamics. Structural heterogeneity creates spatial correlation between SOC inputs, which are concentrated where plant canopies and root systems are present, and soil moisture conditions, which may be made more or less favorable for decomposition by the local presence of vegetation. At Jornada, the modeled average residence time (yr) of SOC, equal to SOC pool size (gC m^{-2}) divided by the input rate (ADD; gC m^{-2} yr^{-1}) for a steady-state system, was 27.6 years for the shrubland and 24.0 years for the grassland (assuming a growing season length of 177 days, for unit conversion from days to years), indicating that the structure of the shrubland slightly decreases decomposition. At Riesel the pattern was more pronounced, with mean residence times of 20.5 years for the shrubland and 15.6 years for the grassland.

[42] Figure 6 shows the distribution of SOC residence times for Jornada and Riesel shrublands as percent deviation from the landscape average. Riesel is much more heterogeneous, because the high vegetation density creates more combinations of overlapping roots, canopies, and grass patches. In both cases there are small pools with very high decomposition rates, but they are countered by large pools with slower than average decomposition rates. As shown in Figure 7, the fastest decomposition rates occur where the number of root systems contributing to uptake is low. At low root densities, the presence of canopies leads to wetter soils, because of the reduction in evaporation. However, at high root densities, root uptake keeps soil moisture at low values

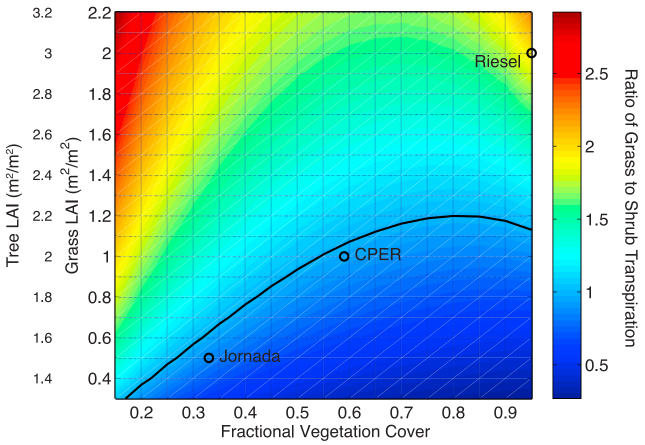

Figure 5. Ratio of landscape average transpiration rate for landscapes containing grass only versus shrubs only over a range of fractional vegetation covers and canopy or grass patch leaf area index values. The black line shows a 1:1 ratio of grassland to shrubland transpiration. Other parameters are mean storm depth α = 7.5 mm, storm frequency λ_s = 0.27 day^{-1}, PET = 4.3 mm d^{-1}, soil parameters for a loamy sand, and general model parameters given in Table 1. Locations of study sites in the parameter space are shown by black circles. Transpiration ratios at these points may differ from site model results because average climate and soil parameters are used.

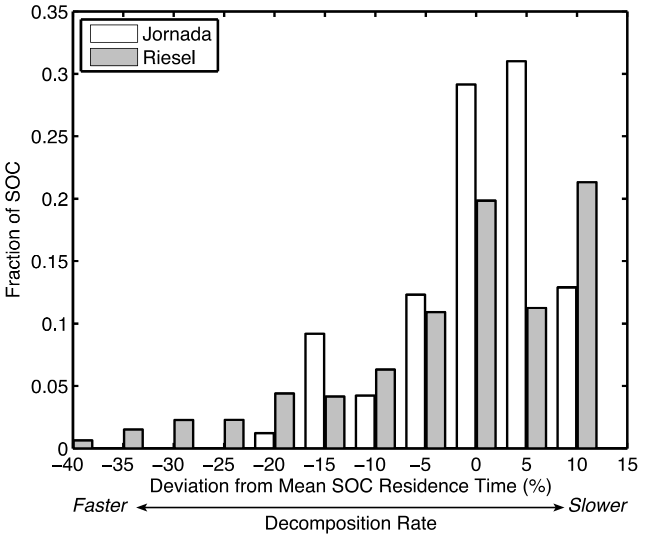

Figure 6. Distribution of SOC residence times at Jornada (white bars) and Riesel (gray bars) shrublands, expressed as the percent deviation from the landscape average. Residence time in each patch type is the modeled SOC pool size divided by the modeled productivity. Distributions are in terms of the fraction of input to pools with a given residence time.

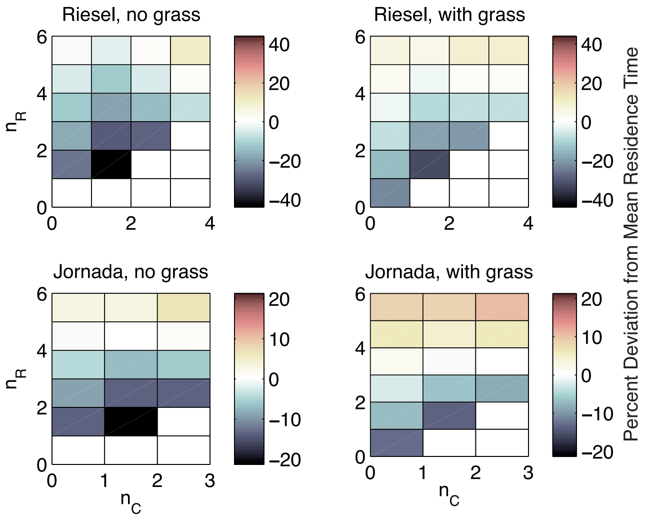

Figure 7. SOC residence times in shrubland vegetation patches as a function of the number of shrub canopies (n_C) and root systems (n_R) overlapping a point for patches also covered by grass or not covered by grass. Residence times are expressed as the percent deviation from the landscape average.

where evaporation is limited by the availability of water rather than the availability of energy. In this case, the role of canopy interception is more important and the presence of canopies leads to drier soil.

4. Discussion

[43] We modeled the coupled soil moisture and carbon cycles of semi-arid grasslands and shrublands, accounting for the local effects of plant canopies and root systems. Our results help to explain why woody encroachment can increase SOC stocks under certain climate, soil, and vegetation conditions but cause a decrease under others. The observed pattern of SOC gain or loss with woody encroachment was driven by the relative difference in productivity between grasslands and shrublands at each site, as the modeled effect on decomposition rates followed the opposite pattern. Most data on the change in productivity associated with woody encroachment include only aboveground net primary productivity. Except at the most arid sites, aboveground productivity increases with woody encroachment, and there is a positive relationship between this increase and MAP [*Knapp et al.*, 2008; *Barger et al.*, 2011], though a relationship between change in aboveground productivity and change in SOC was not shown. Our model predicted a decrease in shrubland productivity relative to grassland productivity with increasing MAP. There are two possible reasons for the discrepancy.

[44] First, the increase in aboveground net primary productivity with woody encroachment observed by *Knapp et al.* [2008] showed a strong positive correlation with an increase in landscape LAI. Some instances of woody encroachment summarized in the meta analysis were estimated to have produced LAI increases of more than 10 m^2 m^{-2}, though results vary with different measurement techniques [*Brantley and Young*, 2007]. The grasslands at the Riesel site are highly productive rangelands [*Guo and Gifford*, 2002], so the predicted increase in landscape LAI with encroachment (1.5 m^2 m^{-2}) was small. The data set used in our analysis showed an increase in SOC stocks with woody encroachment for xeric sites, and a decrease in SOC stocks at more mesic sites. However, more recent studies have found examples of mesic systems in which woody encroachment increased SOC stocks [*McKinley and Blair*, 2008; *Brantley and Young*, 2010]. The native grasslands at these sites, a temperate prairie and a barrier island, were less productive and had lower initial SOC stocks than the Texas rangelands used in the study by *Jackson et al.* [2002]. Our model identifies scenarios in which shrubs have a higher relative LAI as conditions under which shrublands will have higher transpiration and productivity, even at high vegetation densities (Figure 5).

[45] Second, aboveground net primary productivity is not a direct proxy for total net primary productivity. Water-limited ecosystems can have large root biomass pools [*Schulze et al.*, 1996; *Schenk and Jackson*, 2002], which provide input to SOC pools through root turnover. Herbaceous vegetation has been shown to increase belowground allocation with decreasing plant water availability [*Hui and Jackson*, 2006; *Armas and Pugnaire*, 2011]. Theoretical predictions suggest that woody vegetation should follow the same pattern [*Laio et al.*, 2006; *Guswa*, 2008], but a relationship between climate and belowground allocation in woody vegetation has yet to be shown empirically [*Bhattachan et al.*, 2012]. If a shrub community encroaches on a grassland with a higher belowground to aboveground allocation ratio, it could increase aboveground net primary productivity while still decreasing total productivity and SOC stocks. A meta analysis of allocation across biomes found that on average grasses allocate a greater fraction of biomass to roots than shrubs, though there was a large amount of variability in the data [*Poorter et al.*, 2012]. A better understanding of the drivers of belowground allocation in woody plants is needed to predict the conditions under which this could happen.

[46] Most analyses of the spatial heterogeneity of hydrological and biogeochemical cycling in drylands divide the landscape into two categories: under- and inter-canopy [e.g. *Bhark and Small*, 2003; *Hamerlynck et al.*, 2011]. However, conditions of both lower and higher soil moisture under canopies have been observed within the same landscape in the field [*D'Odorico et al.*, 2007; *Cable et al.*, 2012] and in the results of our model. Soil moisture, and thus decomposition rates, in patches classified as "under-canopy" ($n_C \geq 1$ in our model) could be anomalously high or low (Figure 6), depending on the balance of canopy interception, root uptake, and reduced evaporation. An approach like ours that considers the local influence of both canopies and root systems can help to explain the variability in field observations of under-canopy microsites. Other sources of heterogeneity, such as the size and age of the overlapping canopies and root systems, may also be important in determining soil nutrient cycles [*Throop and Archer*, 2008; *Brantley and Young*, 2010].

[47] Modeling the effects of woody encroachment on hydrological dynamics requires that evapotranspiration, which is normally modeled as a single flux, be partitioned into evaporation and transpiration [*Huxman et al.*, 2005; *Moore and Heilman*, 2011]. Our approach, based on the partitioning of incident radiation, is simplistic but produces

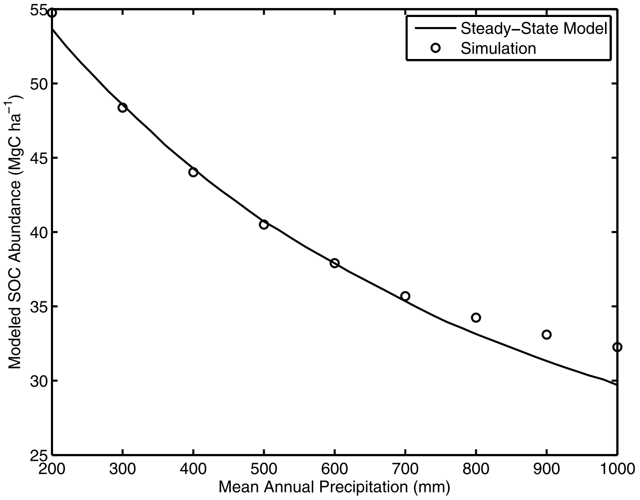

Figure A1. Comparison of the steady-state model of SOC pool size (line) with ensemble averages (N = 10) of a simulated time series (duration 100,000 days) of SOC dynamics forced by a stochastically-generated rainfall pattern (circles) over a gradient of mean annual precipitation. Precipitation was varied by changing rainfall frequency (λ_r), while mean storm depth (α) was held constant at 10 mm. A constant value of 1 gC m^{-2} d^{-1} was used for the SOC addition rate (ADD). The models were parameterized for a spatially homogeneous grass layer on sandy soil with a potential evapotranspiration of 4.3 mm d^{-1}. Other model parameters are given in Table 1.

results that fall well within the range of measured values from studies in the American Southwest reviewed by *Reynolds et al.* [2000]. It could provide a starting point for more detailed models of the effects of woody encroachment on ecosystem water and energy balances. Both are important, as changes in streamflow have been observed where woody encroachment affects a riparian zone [*Wilcox*, 2002], and there is evidence that shrubs facilitate their own establishment and proliferation by increasing surface temperatures [*He et al.*, 2011].

[48] Accurately describing the "sphere of influence" of a root system based on parameters that can be measured aboveground presents a significant challenge. Data on belowground structure, particularly of woody vegetation, are lacking, even though the sensitivity of models to changes in rooting parameters is often high [*Jackson et al.*, 2000]. In a meta analysis of root excavations and isotope tracer studies, *Casper et al.* [2003] found that lateral root spread is roughly proportional to canopy size, with higher lateral spreads observed at dry sites with coarse soils. To reflect these findings, we defined the parameter a_t, the ratio of root system radius to canopy radius, as constant within a landscape. The data necessary to assign site-specific values of a_t based on climate and soil parameters were not available, but the sensitivity of the SOC model to changes in a_t was small. Assigning an increased a_t value of 3.5 to Jornada (the dry site with coarse soil) produced a 4% increase in the shrubland SOC estimate, while reducing the a_t value at Riesel to 1.5 lowered the SOC estimate by 1%. However, the effect of changing a_t produced proportionally larger changes in productivity and SOC residence time. The effects compensated for each other, leading to small changes in modeled SOC. Thus, determining realistic a_t values is necessary to ensuring that the internal dynamics of the model are correct and can accurately predict response to change.

5. Conclusions

[49] We developed a steady-state model of coupled SOC and soil moisture dynamics that accounts for the effects of structural heterogeneity at the scale of vegetation patches. Our temporal averaging approach uses a multiplicative noise model to account for the temporal variability in decomposition rate at the daily scale. The model determines a unique solution for points overlapped by a given number of shrub canopies and root systems with the presence or absence of grass. We used a probabilistic description of vegetation structure to determine landscape averages of the state variables.

[50] We used the model to investigate the mechanisms behind observed patterns of SOC change following woody encroachment. A change in vegetation structure affects both the productivity and decomposition components of the SOC balance, but patterns of SOC abundance are primarily determined by productivity. An increase in transpiration and productivity following woody encroachment is likely under two conditions: (1) low vegetation density, where shrubs spread roots laterally and utilize more soil for uptake, and (2) the LAI of shrub canopies is much higher than that of grass patches and more energy is utilized for transpiration than evaporation. The increase in structural complexity associated with encroachment increased spatial heterogeneity in SOC decomposition environments, with patches of both increased and decreased SOC residence time present in the landscape. The presence of vegetation can lead to higher or lower soil moisture conditions depending on the density of vegetation cover and climatic conditions because root systems and canopies influence the water balance through several mechanisms. At the landscape scale, shrublands concentrated SOC inputs in patches with drier soil, leading to overall lower decomposition rates than in grasslands.

[51] The model presented here provides a framework for representing spatial heterogeneity in hydrological and biogeochemical processes induced by patchy vegetation that is easily upscaled to address landscape-scale issues. Additional work is needed to determine the most accurate description of the spatial extent of the influence of a root system. Though we focused on soil carbon change, our spatial framework may also be useful in evaluating the effect of woody encroachment on other components of the water, energy, and carbon balances.

Appendix A: Comparison of Multiplicative Noise Approach with a Simulation-Based Model

[52] Our steady-state approximation of the dynamics of the SOC pools (equation (15)) using a multiplicative noise model (equation (22)) does not represent temporal autocorrelation of soil moisture values. To ensure that this simplification did not introduce significant bias, we compared our model results to a version of the model that simulates a time series of the state variables forced by a stochastically-generated rainfall record. Figure A1 shows a comparison of the steady-state model with ensemble averages of the simulation-based model over a range of precipitation conditions.

Table B1. Site-Specific Model Parameters for Kalahari Transect Sites Used in Model Verification

Site	Community Type[a]	Storm Frequency (d^{-1})[b]	PET (mm/d)[c]	Shrub Frequency (ind/m^2)[d]	Woody Cover (%)[a]	Grass Cover (%)[e]
1. Mongu, Zambia	Kalahari woodland	0.38	4.9	0.097	64.8	7
2. Senanga, Zambia	Kalahari woodland	0.35	4.9	0.046	53.7	10
3. Sioma, Zambia	Dry Kalahari woodland	0.32	4.9	0.084	61.0	12
4. Katima Mulilo, Zambia	Dry deciduous forest	0.31	4.9	0.017	29.9	15
5. Pandamatenga, Botswana	Dry deciduous forest	0.30	4.9	0.043	32.3	17
6. Maun, Botswana	Mophane woodland	0.20	4.6	0.097	36.1	21
7. Ghanzi, Botswana	Northern Kalahari savanna	0.17	4.6	0.030	32.0	16
8. Gobabis, Namibia	Central Kalahari savanna	0.18	4.4	0.098	19.1	11
9. Tshane, Botswana	Southern Kalahari savanna	0.16	4.3	0.018	13.8	12
10. Upington, South Africa	Arid shrub savanna	0.09	4.3	0.029	5.8	17

[a] *Scholes et al.* [2002].
[b] *Porporato et al.* [2003b].
[c] *Scholes et al.* [2004].
[d] *Caylor et al.* [2003].
[e] *Scanlon et al.* [2002]

The models deviated slightly under very dry and very wet conditions, where extended dry or wet periods increase the temporal autocorrelation of soil moisture. However, the models were in good agreement for the range of MAP values encompassing most semi-arid ecosystems.

Appendix B: Model Verification: The Kalahari Transect

[53] The Kalahari Transect in southern Africa has been a site of intensive research on the biogeochemistry, structure, and function of water-limited ecosystems. The Kalahari sands are deep, homogeneous, sandy soils that span a large gradient in MAP, enabling the study of the links between climate and ecosystem processes without the confounding effect of soil texture [*Scholes and Parsons*, 1997]. Prior work on the Kalahari Transect includes detailed surveys of vegetation structure [*Scholes et al.*, 2002; *Caylor et al.*, 2003], which provide the parameters needed for the SOC model. SOC abundance has also been measured along the transect [*Ringrose et al.*, 1998], making it an ideal site for model verification.

[54] Site-specific model parameters for 10 Kalahari Transect sites are given in Table B1. Sites 4–10 span the same portion of the transect surveyed by *Ringrose et al.* [1998] and are used in the verification of the SOC model (Figure B1). The seven verification sites represent six vegetation community types. All but one of the model estimates fall within the 95% confidence bounds of the field data for the community type they represent.

[55] Long-term data on net primary productivity are not available for the Kalahari, but community-level productivity models have been applied to the region [*Caylor et al.*, 2004; *Woodward and Lomas*, 2004]. We use these to evaluate our simplified representation of productivity as the product of transpiration and water use efficiency (Figure B2). We use sites 1–9 from Table B1, which overlap the portion of the transect analyzed in the other studies. *Caylor et al.* [2004] apply a canopy productivity simulation developed by *Dowty* [1999], which includes mechanistic leaf physiology routines for C_3 and C_4 plants and is forced by daily meteorological data. The study predicted much higher net primary productivity across the transect than *Woodward and Lomas* [2004], who applied the Sheffield Global Dynamic Vegetation Model, a global-scale model that predicts vegetation structure and dynamics from inputs of monthly climate data. Our estimates of net primary productivity fell within the range predicted by the two models for six of nine sites. The broad range of productivity values predicted by physiology models suggests that using a more complex formulation in our model is unlikely to constitute a verifiable improvement.

Appendix C: Effects of Precipitation and Soil Texture on SOC Abundance

[56] We tested the sensitivity of the model to changes in rainfall and soil texture parameters to determine if abiotic

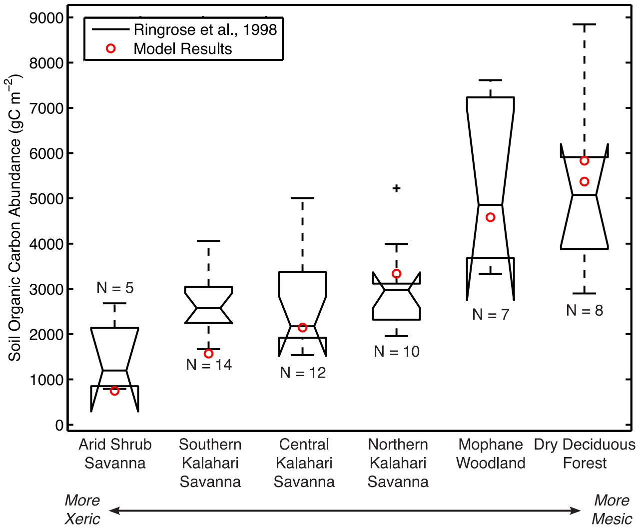

Figure B1. Comparison of SOC model results for seven sites (red circles) on the Kalahari Transect with data from *Ringrose et al.* [1998] (black box plots) from 57 sampling locations, grouped by community type. Notches show 95% confidence intervals for the data, and the number of sampling locations in each community type is given. General model parameters are given in Table 1 and site-specific parameters in Table B1. Results for sites 4–10 from Table B1 are presented. Parameters used for all Kalahari sites are mean storm depth (α; 10 mm), soil texture (sand), shrub canopy leaf area index (LAI_s; 2.0 m^2 m^{-2}), and grass patch leaf area index (LAI_g; 1.0 m^2 m^{-2}).

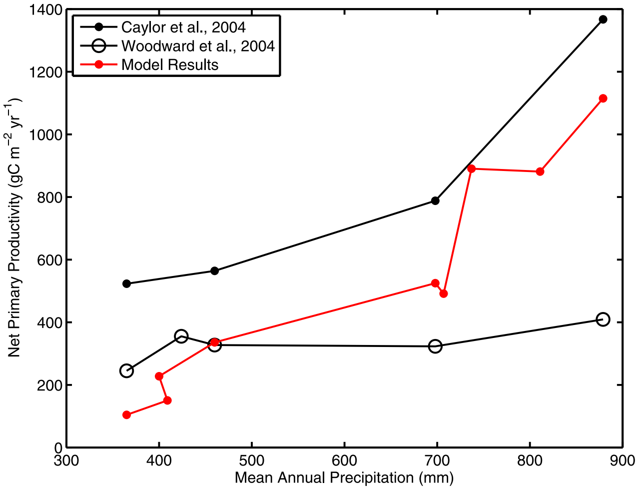

Figure B2. Comparison of results from the net primary productivity component of the SOC model for eight sites (red dots) on the Kalahari Transect with productivity estimates from a canopy physiology simulation model [*Caylor et al.*, 2004] (black dots) and a dynamic global vegetation model [*Woodward and Lomas*, 2004] (black circles) applied to the Kalahari Transect. General model parameters are given in Table 1 and site-specific parameters in Table B1. Results for sites 1–9 from Table B1 are presented. Parameters used for all Kalahari sites are mean storm depth (α; 10 mm), soil texture (sand), shrub canopy leaf area index (LAI_s; 2.0 m^2 m^{-2}), and grass patch leaf area index (LAI_g; 1.0 m^2 m^{-2}).

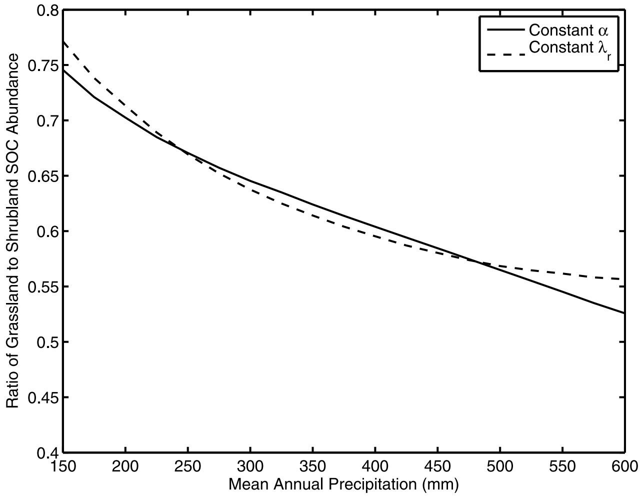

Figure C1. Modeled ratio of grassland SOC stocks to shrubland SOC stocks for paired grassland and shrubland communities at Jornada, NM, across a range of rainfall conditions. The solid line shows the result of holding storm frequency (λ_r) constant at 0.25 d^{-1} while varying mean storm depth (α). The dashed line shows the result of holding mean storm depth constant at 5.2 mm while varying storm frequency. Assuming a growing season length of 175 days, this corresponds to mean annual precipitation values of 160–600 mm. Other model parameters are taken from Tables 1 and 2.

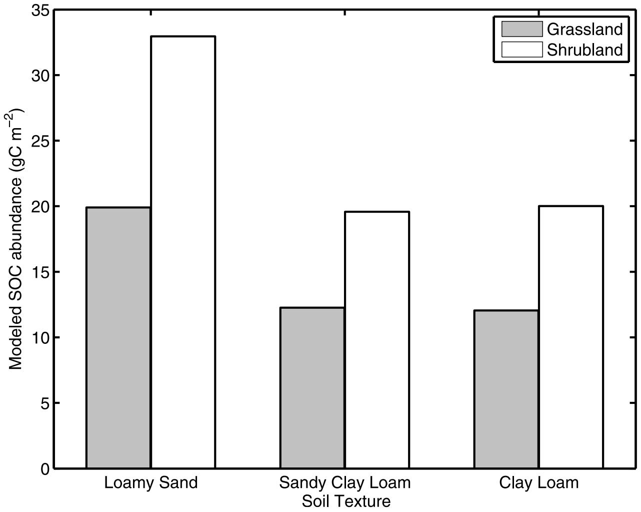

Figure C2. Modeled SOC stocks for paired grassland (gray bars) and shrubland (white bars) communities at Jornada, NM, for three soil textures. The three textures—loamy sand (coarse), sandy clay loam (intermediate), and clay loam (fine)—are observed at Jornada (dry), CPER (intermediate), and Riesel (wet), respectively. Other model parameters are taken from Tables 1 and 2.

factors alone could explain the observed pattern of SOC abundance at the sites in the American Southwest. Increasing rainfall while holding the other parameters constant did not produce a shift towards grass-dominated systems storing more SOC. Figure C1 shows the effect of increasing MAP through either an increase in storm frequency (λ_r) or mean storm depth (α) on the relative SOC abundance in paired grassland and shrubland communities in the arid Jornada landscape. Changing rainfall alone produced the opposite of the pattern observed by *Jackson et al.* [2002], with SOC stocks in the shrubland increasing more with rainfall than those in the grassland.

[57] *Barger et al.* [2011] found a positive relationship between soil clay content and SOC accumulation with woody encroachment. Even though our sites do not reflect this pattern, we ran the model varying only soil texture to determine if it has a direct effect on SOC change. The results of running the SOC model for Jornada but changing the soil texture parameters from loamy sand to sandy clay loam, as occurs at the CPER, or clay loam, as occurs at Riesel, are shown in Figure C2. As with changing rainfall alone, changing soil texture does not produce the observed pattern of relative grassland-shrubland SOC abundance.

[58] **Acknowledgments.** The authors acknowledge the support of Princeton University and the NSF through CAREER grant EAR-847368 and grants DEB-742933 and BCS/EAR-1026334.

References

Ansley, R. J., X. B. Wu, and B. A. Kramp (2001), Observation: Long-term increases in mesquite canopy cover in a North Texas savanna, *J. Range Manage.*, *54*, 171–176, doi:10.2307/4003179.

Archer, S., D. S. Schimel, and E. A. Holland (1995), Mechanisms of shrubland expansion: Land use, climate or CO$_2$?, *Clim. Change*, *29*(1), 91–99, doi:10.1007/BF01091640.

Armas, C., and F. I. Pugnaire (2011), Belowground zone of influence in a tussock grass species, *Acta Oecol.*, *37*(3), 284–289, doi:10.1016/j.actao.2011.02.013.

Aston, A. R. (1979), Rainfall interception by eight small trees, *J. Hydrol.*, *42*, 383–396.

Austin, A. T. (2011), Has water limited our imagination for aridland biogeochemistry?, *Trends Ecol. Evol.*, *26*(5), 229–235, doi:10.1016/j.tree.2011.02.003.

Austin, A. T., and L. Vivanco (2006), Plant litter decomposition in a semiarid ecosystem controlled by photodegradation, *Nature*, *442*, 555–558, doi:10.1038/nature05038.

Austin, A. T., P. I. Araujo, and P. E. Leva (2009), Interaction of position, litter type, and water pulses on decomposition of grasses from the semiarid Patagonian steppe, *Ecology*, *90*(9), 2642–2647, doi:10.1890/08-1804.1.

Bahn, M., et al. (2010), Soil respiration at mean annual temperature predicts annual total across vegetation types and biomes, *Biogeosciences*, *7*(7), 2147–2157, doi:10.5194/bg-7-2147-2010.

Bai, Y., T. Colberg, J. T. Romo, B. McConkey, D. Pennock, and R. Farrell (2009), Does expansion of western snowberry enhance ecosystem carbon sequestration and storage in Canadian prairies?, *Agric. Ecosyst. Environ.*, *134*, 269–276, doi:10.1016/j.agee.2009.07.009.

Barger, N. N., S. A. Archer, J. L. Campbell, C. Huang, J. A. Morton, and A. K. Knapp (2011), Woody plant proliferation in North American drylands: A synthesis of impacts on ecosystem carbon balance, *J. Geophys. Res.*, *116*, G00K07, doi:10.1029/2010JG001506.

Bestelmeyer, B. T., and J. A. Wiens (2001), Ant biodiversity in semiarid landscape mosaics: The consequences of grazing vs. natural heterogeneity, *Ecol. Appl.*, *11*(4), 1123–1140, doi:10.1890/1051-0761(2001)011[1123:ABISLM]2.0.CO;2.

Bhark, E., and E. Small (2003), Association between plant canopies and the spatial patterns of infiltration in shrubland and grassland of the Chihuahuan Desert, New Mexico, *Ecosystems*, *6*(2), 185–196, doi:10.1007/s10021-002-0210-9.

Bhattachan, A., M. Tatlhego, K. Dintwe, F. O'Donnell, K. K. Caylor, G. S. Okin, D. O. Perrot, S. Ringrose, and P. D'Odorico (2012), Evaluating ecohydrological theories of woody root distribution in the Kalahari, *PLoS: ONE*, *7*(3), e33996, doi:10.1371/journal.pone.0033996.

Brantley, S. T., and D. R. Young (2007), Leaf-area index and light attenuation in rapidly expanding shrub thickets, *Ecology*, *88*(2), 524–530.

Brantley, S. T., and D. R. Young (2010), Shrub expansion stimulates soil C and N storage along a coastal soil chronosequence, *Global Change Biol.*, *16*(7), 2052–2061, doi:10.1111/j.1365-2486.2009.02129.x.

Brubaker, K. L., and D. Entekhabi (1996), Analysis of feedback mechanisms in land-atmosphere interaction, *Water Resour. Res.*, *32*(5), 1343–1357, doi:10.1029/96WR00005.

Brutsaert, W. (1982), *Evaporation Into the Atmosphere: Theory, History, and Applications*, D. Reidel, Dordrecht, Netherlands.

Cable, J. M., G. A. Barron-Gafford, K. Ogle, M. Pavao-Zuckerman, R. L. Scott, D. G. Williams, and T. E. Huxman (2012), Shrub encroachment alters sensitivity of soil respiration to temperature and moisture, *J. Geophys. Res.*, *117*(G1), G01001, doi:10.1029/2011JG001757.

Cabon, F., G. Girard, and E. Ledoux (1991), Modelling of the nitrogen cycle in farm land areas, *Fertilizer Res.*, *27*(2–3), 161–169, doi:10.1007/BF01051124.

Casper, B. B., H. J. Schenk, and R. B. Jackson (2003), Defining a plant's belowground zone of influence, *Ecology*, *84*(9), 2313–2321.

Caylor, K. K., H. H. Shugart, P. R. Dowty, and T. M. Smith (2003), Tree spacing along the Kalahari Transect in southern Africa, *J. Arid Environ.*, *54*(2), 281–296, doi:10.1006/jare.2002.1090.

Caylor, K. K., P. R. Dowty, H. H. Shugart, and S. Ringrose (2004), Relationship between small-scale structural variability and simulated vegetation productivity across a regional moisture gradient in southern Africa, *Global Change Biol.*, *10*, 374–382, doi:10.1046/j.1529-8817.2003.00704.x.

Caylor, K. K., P. D'Odorico, and I. Rodriguez-Iturbe (2006), On the ecohydrology of structurally heterogeneous semiarid landscapes, *Water Resour. Res.*, *42*, W07424, doi:10.1029/2005WR004683.

Clapp, R. B., and G. M. Hornberger (1978), Empirical equations for some soil hydraulic properties, *Water Resour. Res.*, *14*(4), 601–604, doi: doi:10.1029/WR014i004p00601.

Davidson, E., I. Janssens, and Y. Luo (2006), On the variability of respiration in terrestrial ecosystems: moving beyond Q_{10}, *Global Change Biol.*, *12*(2), 154–164, doi:10.1111/j.1365-2486.2005.01065.x.

Derner, J. D., and X. B. Wu (2004), Spatial patterns of light gaps in mesic grasslands, *J. Range Manage.*, *57*(4), 393–398, doi:10.2307/4003864.

D'Odorico, P., F. Laio, A. Porporato, and I. Rodriguez-Iturbe (2003), Hydrologic controls on soil carbon and nitrogen cycles. II. A case study, *Adv. Water Resour.*, *26*(1), 59–70, doi:10.1016/S0309-1708(02)00095-7.

D'Odorico, P., K. Caylor, G. S. Okin, and T. M. Scanlon (2007), On soil moisture–vegetation feedbacks and their possible effects on the dynamics of dryland ecosystems, *J. Geophys. Res.*, *112*, G04010, doi:10.1029/2006JG000379.

Dowty, P. R. (1999), Modeling biophysical processes in the savannas of Southern Africa, PhD diss., Univ. of Virginia, Charlottesville.

Gibbens, R. (1996), Structure and function of C_3 and C_4 Chihuahuan desert plant communities, standing crop and leaf area index, *J. Arid Environ.*, *34*(1), 47–62, doi:10.1006/jare.1996.0092.

Glenn, E. P., K. Morino, K. Didan, F. Jordan, K. C. Carroll, P. L. Nagler, K. Hultine, L. Sheader, and J. Waugh (2008), Scaling sap flux measurements of grazed and ungrazed shrub communities with fine and coarse-resolution remote sensing, *Ecohydrology*, *1*(4), 316–329, doi:10.1002/eco.v1:4.

Gonzalez-Polo, M., and A. T. Austin (2009), Spatial heterogeneity provides organic matter refuges for soil microbial activity in the Patagonian steppe, Argentina, *Soil Biol. Biochem.*, *41*(6), 1348–1351, doi:10.1016/j.soilbio.2009.03.008.

Goodale, C. L., and E. A. Davidson (2002), Carbon cycle: Uncertain sinks in the shrubs, *Nature*, *418*, 593–594, doi:10.1038/418593a.

Grace, J., J. S. Jose, P. Meir, H. S. Miranda, and R. A. Montes (2006), Productivity and carbon fluxes of tropical savannas, *J. Biogeogr.*, *33*(3), 387–400, doi:10.1111/jbi.2006.33.issue-3.

Guo, L. B., and R. M. Gifford (2002), Soil carbon stocks and land use change: A meta analysis, *Global Change Biol.*, *8*(4), 345–360, doi:10.1046/j.1354-1013.2002.00486.x.

Gusman, A. J., and M. A. Marino (1999), Analytical modeling of nitrogen dynamics in soils and ground water, *J. Irrig. Drain. Eng.*, *125*(6), 330–337, doi:10.1061/(ASCE)0733-9437(1999)125:6(330).

Guswa, A. J. (2008), The influence of climate on root depth: A carbon cost-benefit analysis, *Water Resour. Res.*, *44*, W02427, doi:10.1029/2007WR006384.

Hamerlynck, E. P., R. L. Scott, M. S. Moran, A. M. Schwander, E. Connor, and T. E. Huxman (2011), Inter- and under-canopy soil water, leaf-level and whole-plant gas exchange dynamics of a semi-arid perennial C_4 grass, *Oecologia*, *165*(1), 17–29, doi:10.1007/s00442-010-1757-3.

Harmel, R. D., C. W. Richardson, K. W. King, and P. M. Allen (2006), Runoff and soil loss relationships for the Texas Blackland Prairies ecoregion, *J. Hydrol.*, *331*(3–4), 471–483, doi:10.1016/j.jhydrol.2006.05.033.

Hazlett, D. L. (1992), Leaf area development of four plant communities in the Colorado steppe, *Am. Midland Nat.*, *127*(2), 276–289.

He, Y., S. DeWekker, J. D. Fuentes, and P. D'Odorico (2011), Coupled land-atmosphere modeling of the effects of shrub encroachment on nighttime temperatures, *Agric. For. Meteorol.*, *151*, 1690–1697, doi:10.1016/j.agrformet.2011.07.005.

Hibbard, K. A., D. S. Schimel, S. Archer, D. S. Ojima, and W. Parton (2003), Grassland to woodland transitions: Integrating changes in landscape structure and biogeochemistry, *Ecol. Appl.*, *13*(4), 911–926.

Hook, P. B., and I. C. Burke (2000), Biogeochemistry in a shortgrass landscape: Control by topography, soil texture, and microclimate, *Ecology*, *81*(10), 2686–2703, doi:10.2307/177334.

House, J. I., S. Archer, D. D. Breshears, and R. J. Scholes (2003), Conundrums in mixed woody-herbaceous plant systems, *J. Biogeogr.*, *30*(11), 1763–1777, doi:10.1046/j.1365-2699.2003.00873.x.

Howes, D. A., and A. D. Abrahams (2003), Modeling runoff and runon in a desert shrubland ecosystem, Jornada Basin, New Mexico, *Geomorphology*, *53*(1–2), 45–73, doi:10.1016/S0169-555X(02)00347-1.

Hui, D., and R. B. Jackson (2006), Geographical and interannual variability in biomass partitioning in grassland ecosystems: A synthesis of field data, *New Phytol.*, *169*(1), 85–93, doi:10.1111/nph.2006.169.issue-1.

Huxman, T. E., B. P. Wilcox, D. D. Breshears, R. L. Scott, K. A. Snyder, E. E. Small, K. Hultine, W. T. Pockman, and R. B. Jackson (2005), Ecohydrological implications of woody plant encroachment, *Ecology*, *86*(2), 308–319.

Jackson, R., J. Canadell, J. Ehleringer, and H. Mooney (1996), A global analysis of root distributions for terrestrial biomes, *Oecologia*, *108*, 389–411.

Jackson, R. B., et al. (2000), Belowground consequences of vegetation change and their treatment in models, *Ecol. Appl.*, *10*(2), 470–483.

Jackson, R. B., J. L. Banner, E. G. Jobbagy, W. T. Pockman, and D. H. Wall (2002), Ecosystem carbon loss with woody plant invasion of grasslands, *Nature*, *418*, 623–626, doi:10.1038/nature00910.

Jarvis, P., et al. (2007), Drying and wetting of Mediterranean soils stimulates decomposition and carbon dioxide emission: The "Birch effect", *Tree Physiol.*, *27*, 929–940.

Jenerette, G. D., R. L. Scott, and T. E. Huxman (2008), Whole ecosystem metabolic pulses following precipitation events, *Funct. Ecol.*, *22*(5), 924–930, doi:10.1111/j.1365-2435.2008.01450.x.

Kieft, T. L., C. S. White, S. R. Loftin, R. Aguilar, J. A. Craig, and D. A. Skaar (1998), Temporal dynamics in soil carbon and nitrogen resources at a grassland-shrubland ecotone, *Ecology*, *79*(2), 671–683, doi:10.2307/176962.

Knapp, A. K., et al. (2008), Shrub encroachment in North American grasslands: Shifts in growth form dominance rapidly alters control of ecosystem carbon inputs, *Global Change Biol.*, *14*(3), 615–623, doi:10.1111/gcb.2008.14.issue-3.

Kulmatiski, A., K. H. Beard, R. J. T. Verweij, and E. C. February (2010), A depth-controlled tracer technique measures vertical, horizontal and temporal patterns of water use by trees and grasses in a subtropical savanna, *New Phytol.*, *188*, 199–209.

Laio, F., A. Porporato, L. Ridolfi, and I. Rodriguez-Iturbe (2001a), Plants in water-controlled ecosystems: Active role in hydrologic processes and response to water stress II. Probabilistic soil moisture dynamics, *Adv. Water Resour.*, *24*, 707–723, doi:10.1016/S0309-1708(01)00005-7.

Laio, F., A. Porporato, C. P. Fernandez-Illescas, and I. Rodriguez-Iturbe (2001b), Plants in water-controlled ecosystems: Active role in hydrologic processes and response to water stress IV. Discussion of real cases, *Adv. Water Resour.*, *24*, 745–762, doi:10.1016/S0309-1708(01)00007-0.

Laio, F., P. D'Odorico, and L. Ridolfi (2006), An analytical model to relate the vertical root distribution to climate and soil properties, *Geophys. Res. Lett.*, *33*, L18401, doi:10.1029/2006GL027331.

Liu, F., X. B. Wu, E. Bai, T. W. Boutton, and S. R. Archer (2010), Spatial scaling of ecosystem C and N in a subtropical savanna landscape, *Global Change Biol.*, *16*(8), 2213–2223, doi:10.1111/j.1365-2486.2009.02099.x.

Manzoni, S., and A. Porporato (2009), Soil carbon and nitrogen mineralization: Theory and models across scales, *Soil Biol. Biochem.*, *41*(7), 1355–1379, doi:10.1016/j.soilbio.2009.02.031.

McCulley, R. L., E. G. Jobbágy, W. T. Pockman, and R. B. Jackson (2004), Nutrient uptake as a contributing explanation for deep rooting in arid and semi-arid ecosystems, *Oecologia*, *141*(4), 620–628, doi:10.1007/s00442-004-1687-z.

McKinley, D. C., and J. M. Blair (2008), Woody plant encroachment by *Juniperus virginiana* in a mesic native grassland promotes rapid carbon and nitrogen accrual, *Ecosystems*, *11*(3), 454–468, doi:10.1007/s10021-008-9133-4.

Moore, G. W., and J. L. Heilman (2011), Proposed principles governing how vegetation changes affect transpiration, *Ecohydrology*, *4*(3), 351–358, doi:10.1002/eco.232.

Morgan, J. A., D. G. Milchunas, D. R. LeCain, M. West, and A. R. Mosier (2007), Carbon dioxide enrichment alters plant community structure and accelerates shrub growth in the shortgrass steppe, *Proc. Nat. Acad. Sci. U.S.A.*, *104*(37), 14,724–14,729, doi:10.1073/pnas.0703427104.

Norris, M. D., J. M. Blair, L. C. Johnson, and R. B. McKane (2001), Assessing changes in biomass, productivity, and C and N stores following *Juniperus virginiana* forest expansion into tallgrass prairie, *Can. J. For. Res.*, *31*, 1940–1946, doi:10.1139/cjfr-31-11-1940.

Parton, W. J., D. S. Ojima, and D. S. Schimel (1994), Environmental change in grasslands: Assessment using models, *Clim. Change*, *28*(1–2), 111–141, doi:10.1007/BF01094103.

Petersen, J. L., and D. N. Ueckert (2005), Fourwing saltbush seed yield and quality: Irrigation, fertilization, and ecotype effects, *Rangeland Ecol. Manage.*, *58*, 299–307, doi:10.2111/1551-5028(2005)58[299:FSSYAQ]2.0.CO;2.

Poorter, H., K. J. Niklas, P. B. Reich, J. Oleksyn, P. Poot, and L. Mommer (2012), Biomass allocation to leaves, stems and roots: Meta-analyses of interspecific variation and environmental control, *New Phytol.*, *193*, 30–50, doi:10.1111/j.1469-8137.2011.03952.x.

Porporato, A., P. D'Odorico, F. Laio, and I. Rodriguez-Iturbe (2003a), Hydrologic controls on soil carbon and nitrogen cycles. I. Modeling scheme, *Adv. Water Resour.*, *26*, 45–58, doi:10.1016/S0309-1708(02)00094-5.

Porporato, A., F. Laio, L. Ridolfi, K. K. Caylor, and I. Rodriguez-Iturbe (2003b), Soil moisture and plant stress dynamics along the Kalahari precipitation gradient, *J. Geophys. Res.*, *108*(D3), 4127, doi:10.1029/2002JD002448.

Reichstein, M., et al. (2003), Modeling temporal and large-scale spatial variability of soil respiration from soil water availability, temperature and vegetation productivity indices, *Global Biogeochem. Cycles*, *17*(4), 1104, doi:10.1029/2003GB002035.

Reynolds, J. F., P. R. Kemp, and J. D. Tenhunen (2000), Effects of long-term rainfall variability on evapotranspiration and soil water distribution in the Chihuahuan Desert: A modeling analysis, *Plant Ecol.*, *150*(1/2), 145–159, doi:10.1023/A:1026530522612.

Ringrose, S., W. Matheson, and C. Vanderpost (1998), Analysis of soil organic carbon and vegetation cover trends along the Botswana Kalahari Transect, *J. Arid Environ.*, *38*(3), 379–396.

Rodriguez-Iturbe, I., D. Entekhabi, and R. L. Bras (1991), Nonlinear dynamics of soil moisture at climate scales: 1. Stochastic analysis, *Water Resour. Res.*, *27*(8), 1899–1906, doi:doi:10.1029/91WR01035.

Rodriguez-Iturbe, I., A. Porporato, and L. Ridolfi (1999), Probabilistic modelling of water balance at a point: The role of climate, soil and vegetation, *Proc. R. Soc. A*, *455*, 3789–3805.

Rutledge, S., D. I. Campbell, D. Baldocchi, and L. A. Schipper (2010), Photodegradation leads to increased carbon dioxide losses from terrestrial organic matter, *Global Change Biol.*, *16*(11), 3065–3074, doi:10.1111/j.1365-2486.2009.02149.x.

Savabi, M., J. Arnold, C. Richardson, and J. L. Krishna (1989), Modeling the effect of brush control on rangeland water yield, *J. Am. Water Resour. Assoc.*, *25*(4), 855–865, doi:10.1111/jawr.1989.25.issue-4.

Scanlon, T. M., J. D. Albertson, K. K. Caylor, and C. A. Williams (2002), Determining land surface fractional cover from NDVI and rainfall time series for a savanna ecosystem, *Remote Sens. Environ.*, *82*, 376–388.

Schenk, H. J., and R. B. Jackson (2002), Rooting depths, lateral root spreads and below-ground/above-ground allometries of plants in water-limited ecosystems, *J. Ecol.*, *90*, 480–494.

Schlesinger, W. H., J. F. Reynolds, G. L. Cunningham, L. F. Huenneke, W. M. Jarrell, R. A. Virginia, and W. G. Whitford (1990), Biological feedbacks in global desertification, *Science*, *247*, 1043–1048, doi:10.1126/science.247.4946.1043.

Scholes, R., and D. A. B. Parsons (1997), *The Kalahari Transect: Research on Global Change and Sustainable Development in Southern Africa, International Global Biosphere Project Report 42*, Secretariat, Stockholm.

Scholes, R., and B. Walker (1993), *An African Savanna: Synthesis of the Nylsvley Study*, Cambridge Univ. Press, Cambridge, U. K.

Scholes, R., P. Dowty, K. Caylor, D. Parsons, P. Frost, and H. Shugart (2002), Trends in savanna structure and composition along an aridity gradient in the Kalahari, *J. Veg. Sci.*, *13*(3), 419–428.

Scholes, R. J., P. G. H. Frost, and Y. Tian (2004), Canopy structure in savannas along a moisture gradient on Kalahari sands, *Global Change Biol.*, *10*, 292–302, doi:10.1046/j.1529-8817.2003.00703.x.

Schulze, E. D., et al. (1996), Rooting depth, water availability, and vegetation cover along an aridity gradient in Patagonia, *Oecologia*, *108*(3), 503–511, doi:10.1007/BF00333727.

Throop, H. L., and S. R. Archer (2008), Shrub (*Prosopis velutina*) encroachment in a semidesert grassland: Spatial-temporal changes in soil organic carbon and nitrogen pools, *Global Change Biol.*, *14*(10), 2420–2431, doi:10.1111/j.1365-2486.2008.01650.x.

Van Auken, O. W. (2000), Shrub invasions of North American semiarid grasslands, *Annu. Rev. Ecol. Syst.*, *31*, 197–215, doi:10.1146/annurev.ecolsys.31.1.197.

Wang, L., P. D'Odorico, S. Manzoni, A. Porporato, and S. Macko (2009), Soil carbon and nitrogen dynamics in southern African savannas: The effect of vegetation-induced patch-scale heterogeneities and large scale rainfall gradients, *Clim. Change*, *94*, 63–76, doi:10.1007/s10584-009-9548-8.

Wilcox, B. P. (2002), Shrub control and streamflow on rangelands: A process based viewpoint, *J. Range Manage.*, *55*(4), 318–326.

Woodbury, P., J. Smith, and L. Heath (2007), Carbon sequestration in the U.S. forest sector from 1990 to 2010, *For. Ecol. Manage.*, *241*, 14–27, doi:10.1016/j.foreco.2006.12.008.

Woodward, F. I., and M. R. Lomas (2004), Simulating vegetation processes along the Kalahari Transect, *Global Change Biol.*, *10*(3), 383–392, doi:10.1046/j.1365-2486.2003.00697.x.

Xu, L., and D. D. Baldocchi (2004), Seasonal variation in carbon dioxide exchange over a Mediterranean annual grassland in California, *Agric. For. Meteorol.*, *123*(1–2), 79–96, doi:10.1016/j.agrformet.2003.10.004.